Uncertainty assessment of digital image correlation method in dynamic applications

Emanuele Zappa, Paolo Mazzoleni, Ali Matinmanesh *

Politecnico di Milano, Dipartimento di Meccanica, via La Masa 1, 20156 Milano, Italy

1. Introduction

Over the recent years, optical full field measurement methods have been widely used in experimental mechanics. The main techniques are photoelasticity, moiré, holographic and speckle interferometry, grid method and digital image correlation (DIC) [1–6]. Digital image correlation [7,8] is a powerful technique, which has been mostly used in static applications. A group of articles have focused on quantification of performances of this method [9–36]. They perform the uncertainty assessment by analyzing either the deformed images acquired experimentally or the synthetic images obtained numerically. These studies are conducted in static conditions.

More recently, in some researches, DIC has been implemented also in dynamic applications such as mode shape recognition and vibration analysis [40–47]. Although some of these studies have performed an uncertainty analysis of the measurement in that particular application [37–47], there seems to be an absolute need of further investigations of DIC performances, to analyze the measuring uncertainty in generic dynamic conditions. The performances of DIC technique, depends on a set of static and dynamic parameters; the former include: image resolution and blurring, lighting conditions and processing parameters. As for the dynamics, the motion parameters (mainly the instantaneous velocity) and the shutter time are usually considered relevant in image-base measurement uncertainty assessment [9,10].

In dynamics, dealing with a moving target, causes a motion effect (i.e. blurring) on the acquired images. This motion effect would not exist, if the acquisition was instantaneous but in reality it is not a valid assumption to be made. The so called exposure time or the effective duration that a camera's shutter is open, is usually not negligible in respect to the velocity of the target. This means that the target slightly displaces during the exposure time which makes a single dot on the target to appear as a stripe on the acquired image. This factor is an important source of uncertainty that needs to be quantified. Therefore, the present study aims to perform a systematic uncertainty assessment of DIC method in general dynamic applications. The study focuses on 2D DIC. In the case of 3D DIC similar problems will arise and therefore, a complete understanding of two dimensional conditions will be of great help to further studies which deal with 3D conditions.

To analyze the effect of dynamics on the DIC uncertainty a numerical and experimental approach is proposed in this work. The use of a numerical technique, capable to simulate the effect of the motion on acquired images, allows us to keep all the other uncertainty sources under control and to explore the effect of

* Corresponding author. Tel.: +39 380 181 2779.
  E-mail address: ali.matin@mail.polimi.it (A. Matinmanesh).

dynamics. With this model and a given image of the target, it is possible to simulate the dynamic test and create a set of images that simulate the ones that would be obtained from a real test, with a known imposed vibration law. Analyzing the simulated image set by means of a digital image algorithm and comparing the obtained results with the known imposed motion law, the motion induced uncertainty can be easily quantified.

Moreover, set of experimental tests were conducted aiming first to validate the results obtained from the introduced numerical simulation procedure and second to perform an experimental uncertainty assessment. Results of this part show good agreement between the experiments and the simulations, proving the introduced technique to be an effective method for motion induced uncertainty estimation.

2. State of the art

Studying the uncertainty of DIC in static applications started early on and remarkable advances have been made in this area especially in the recent years. Schreier et al. analyzed the systematic error that arises from the use of under matched shape function, i.e. shape functions of lower order than the actual displacement field. They showed that, under certain conditions, the shape functions used can be approximated by a Savitzky–Golay low-pass filter applied to the displacement functions, permitting a convenient error analysis. They also claimed that, this analysis is not limited to the displacements, but also extends to strain's systematic errors associated with an under matched shape function [11].

The sensitivity of displacement evaluation to the image acquisition noise (e.g. digitization, read-out noise, black current noise, photon noise [12]) were analyzed for the first time in Refs. [13,14]. Their analysis was based on corrupting reference image by different levels of zero mean Gaussian noise and without superimposing any displacement field on the image. They demonstrated that the standard deviation of the displacement error is proportional to the standard deviation of the image noise, and inversely proportional to the average of the squared grey level gradients and to the subset size. These results were also approved later on Refs. [15,16,17]. Wang et al. proposed a method to estimate the DIC error caused by intensity pattern noise [15] and reached to the same conclusion as in Refs. [13,14]. Later, Wang et al. quantified the expectation (bias) and variance in image motions in the presence of uncorrelated Gaussian intensity noise for each pixel location as a function of: interpolation method, sub-pixel motion, intensity noise, contrast, level of uniaxial normal strain and subset size. Their theoretical results in both cases of 1D and 2D showed that the expectations for the local parameters are biased and a function of: the interpolation difference between the translated and reference images, the magnitude of white noise, the decimal part of the motion and the intensity pattern gradients. They demonstrated that adding noise increases the systematic error amplitude [16,17].

Several studies performed an experimental uncertainty assessment and highlighted the influence of hardware, acquisition system, experimental condition and set up on DIC accuracy and precision. Um et al. experimentally obtained the correlation error distributions around the hole in a paper tensile specimen at three different load levels [18]. In the same year, Siebert et al. investigated the impact of facet (sub-image) size and camera noise on correlation error. They demonstrated that decreasing camera noise or increasing the facet size will reduce the correlation error [19]. In the same year, Tiwari et al. obtained the effect of image distortions type on variability and accuracy of ultra high speed and moderate speed image acquisition. They demonstrated that

image correlation measurements using high speed imaging systems are unbiased and consistent with independent deformation measurements over the same length scale, with point-to-point strain variations that are similar to results obtained from translation experiments [20]. A year later, Haddadi et al. proposed numerical and experimental tests, based on rigid-body motion in order to quickly assess the errors related to lighting, the optical lens (distortion), the CCD sensor, the out-of-plane displacement, the speckle pattern, the grid pitch, the size of the subset and the correlation algorithm [21]. More recently, Lava et al. and Pan et al. investigated the impact of lens distortion on the uncertainty of DIC measurement [22,23].

Some efforts have been made to theoretically estimate the DIC uncertainty. Reu et al. quantitatively calculated the errors which will result from any given set of real images obtained in an experiment and concluded that the bias errors can be minimized by selecting higher ordered shape functions, increasing image contrast, and selecting a subset with adequate information content and suggested that the variance parameter can be minimized by decreasing intensity noise in the images which can be accomplished either through better imaging equipment, improved illumination, lower camera gain, or by averaging multiple images at each step. They showed that increasing the subset size up to a given threshold decreases the displacement bias error [24]. In the same year, Pan et al. investigated the influence of the speckle patterns on the accuracy and precision of displacement measurement. They derived a concise theoretical model, which indicates that the speckle pattern does not introduce systematic error but introduce random error in the measured displacement. Their Numerical experiments allowed them to conclude that the standard deviation error of measured displacement is closely related to the speckle patterns [25]. In a more recent study, Crammond et al. investigated the effect of speckle size and density on the uncertainty of measurement [26].

Group of studies investigated DIC uncertainty by creating set of synthetic images. In Refs. [27,28] the displacement error assessment was studied by generating synthetic speckle images, assuming a sinusoidal displacement field with various frequencies and amplitudes. Their results showed the general trends, rather independent of the implementations but strongly correlated with the assumptions of the underlying algorithms. They discussed various error regimes caused by parameters such as subset size, gray level interpolation, encoding image parameters or shape functions. In another interesting approach, Lava et al. investigated the impact of the adopted correlation function, the interpolation order, the shape function and the subset size on the systematic error mean and standard deviation. They analyzed numerically deformed images obtained by imposing finite element displacement field on an un-deformed image and proved that applying Gaussian smoothing, significantly decreases the systematic error amplitude [29]. In a study on the impact of a non-perpendicular camera alignment to a planar sheet metal specimen's surface, Lava et al. estimated errors by numerically rotating deformed images [30]. Other works [31,32] focused on errors that can be directly attributed to the derivation of the strain fields, such as the strain-window size and the strain-window interpolation order using the same technique. Wang et al. by performing numerical 2D DIC tests on the deformation of numerically deformed images, taken from the real tensile specimens, found that the DIC accuracy and precision decrease under highly heterogeneous strain states. They also studied impacts of subset sizes, step sizes and strain window sizes for an optimum correlation [32]. More recently, some efforts have been done to reduce the estimation error in incremental DIC by means of adaptive subset offset [33].

There are some which studies which focus on the uncertainty estimation in 3D such as Refs. [34,35,36], but since the present

work only deals with two dimensional analysis they will not be discussed here.

2.1. Implementing DIC in dynamic applications

Although, the above mentioned works mostly concerned static cases, the implementation of DIC did not remain limited to static applications. Schmidt et al. implemented digital image correlation technique in two dynamic applications. The first application aimed to utilize short-duration white light pulses for studying the automobile tires on road and the second one was an initial work with a pulsed laser to study a flywheel in a spin pit [37,38]. Later on, Kirugulige at al. investigated the dynamic crack growth behavior of a polymeric beam that was subjected to impact loading using developed DIC methodology [39]. Recently, DIC have been applied also to the problem of modal analysis and vibration measurement. In this group of studies, the results of DIC measurement have been compared with the results obtained from accelerometers, scanning laser vibrometer or a finite element model [40–47].

To the best of our knowledge, no researches have focused on systematic uncertainty assessment of digital image correlation method in dynamic conditions, which is the aim of this work.

2.2. Simulation of images with sub-pixel translation

Part of the current work focuses on simulation of images with motion effect acquired in a real dynamic test. The motion simulation technique which is introduced here is based on simulating images with pure translation; therefore a brief discussion on available sub-pixel shifting methods seems to be essential.

In order to create sub-pixel shifted images different techniques were introduced in the literature. Reu introduced an experimental method to create sub-pixel shifted images using a high-resolution camera and the pure decimation scheme [48]. In another work he suggested to use numerical binning rather than a pure decimation scheme in order to avoid aliasing and to more accurately replicate the way a digital camera works [49]. The proposed method was based on oversampling of un-deformed image and generation of reference and deformed image by pixel binning. Wattrisse et al. [50] and Zhou et al. [51] have proposed to define the analytic speckle function as a sum of individual Gaussian-shaped speckles for the purpose of testing their own DIC codes. This kind of synthetic images has also been exploited more recently [52–54]. For example, Pan et al. created a function where the speckle size and distribution can be controlled; this function can then be sampled to create a speckle image with any translation or strain [52]. Orteu proposed a simulation scheme which seeks to capture the experimental aspects of the detector, including noise and photo-diode fill factor [55]. Lava et al. created a method of overlaying a speckle pattern onto deformations calculated via FE software, again, for the evaluation of 2D correlation methods [29]. Fourier shifting is also one of the numerical methods that is claimed to be the optimum sub pixel shifting technique by Reu [49]. This technique will be discussed in details in Section 3.1.

3. Methods

In order to analyze the uncertainty of DIC in dynamic conditions, a set of reference images of a target are required; the current section describes the numerical and experimental approaches which were applied to obtain this image set. At first, image sub pixel translation by means of discrete Fourier transform (DFT) phase shift [49] is recalled because this operation is required in the introduced method to simulate the motion effect. Next, the

experimental procedure and tests' set up are explained and finally the implemented method for simulation of acquired images in a vibration testis revealed.

3.1. Sub pixel shift using DFT

Simulation of pure translation is the first step towards simulating the motion effect as will be explained in Section 3.2. As it was mentioned in Section 2, in order to create sub-pixel shifted images different methods were introduced in the literature. Fourier shifting is one of them that is shown to be the best sub pixel shifting technique by Reu [49].This technique is based on convolving the image with a shifted impulse function and is composed of three simple steps. The image is first transformed in to the frequency domain via discrete Fourier transform (DFT). Then, a linear phase shift (i.e. with a phase shift linearly proportional to the spatial frequency) is applied in the complex plane. The amount of added phase determines the amount of the spatial shift. Finally the image is transformed back to the spatial domain via an inverse Fourier transform. The transforms are done via 1DDFT of one row or one column at a time [49].

It is important to emphasize on the fact that the convolution of the image with a shifted impulse function in the spatial domain would allow only the simulation of integer pixel displacements and thus this shifting technique has been implemented in the frequency domain by Reu [49].

The reference images used in this work, were composed of an unfiltered and a filtered 2000×2000 pixel speckle pattern designed to obtain the best possible performances in terms of DIC uncertainty; relying on literature information (see additional Refs. [51], [56] and [57]).While there are no universal mathematical formulations to define effective speckle patterns, numerous studies have highlighted important characteristics. It is known that an average speckle diameter of a few pixels (e.g. 2–5 pixel [51], 3 pixel [56], 5–7 pixel [57]) is needed to minimize aliasing effects in the correlation analysis while ensuring a good spatial resolution. In the current study in particular a mean speckle diameter of 4.5 pixel and an average on-center spacing of 6 pixel were selected. Moreover a high contrast image was produced, in order to reduce as much as possible the expected uncertainty (see Ref. [17]).

To generate the mentioned reference image, a $20,000 \times 20,000$ image was first created, with 45 pixel diameter circular dots arranged in a regular grid with on-center spacing of 60 pixel. Then, each of the two-dimensional orthogonal coordinates of the centroid of each speckle is perturbed by adding an integer displacement, thus avoiding image resampling. The integer value is randomly extracted from a uniform distribution in the ± 25 pixel range to create a random pattern and to limit speckle superposition. Finally, the 2000×2000 pixel reference image was produced by low-pass anti-aliasing filtering and down sampling by ten times the original high-resolution speckle pattern. Due to this generation technique the frequency content of the non-filtered reference image is limited by the anti-aliasing filter applied prior to down-sampling.

Working on an unfiltered and a filtered reference image allows analyzing the DIC behavior on both very well-focused images (i.e. the basically theoretical images) and on slightly blurred ones (i.e. images with a blurring level that can simulate real acquisition conditions). Fig. 1 shows the reference images. The filtered image is obtained after filtering the unfiltered one by a low pass Gaussian filter with standard deviation of 0.75 pixel.

In order to check the performance of the DFT sub pixel shifting method, the procedure explained above is performed on the reference images shown in Fig. 1, numerically simulating a rigid motion of the target from 0 to 1 pixel with a 0.1 pixel step. Fig. 2 represents the result of digital image correlation analysis
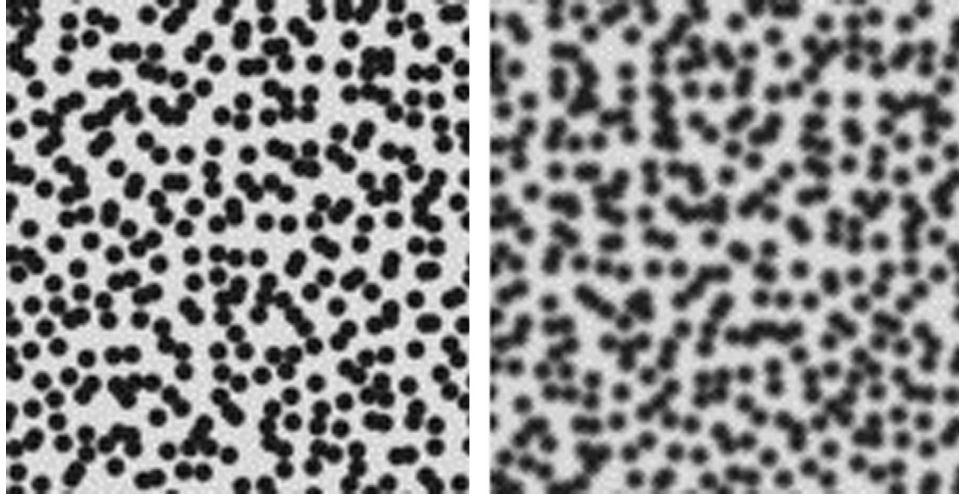
Fig. 1. Part of the reference image before filtering (left) and after filtering with a low pass Gaussian filter with standard deviation of 0.75 pixel (right).
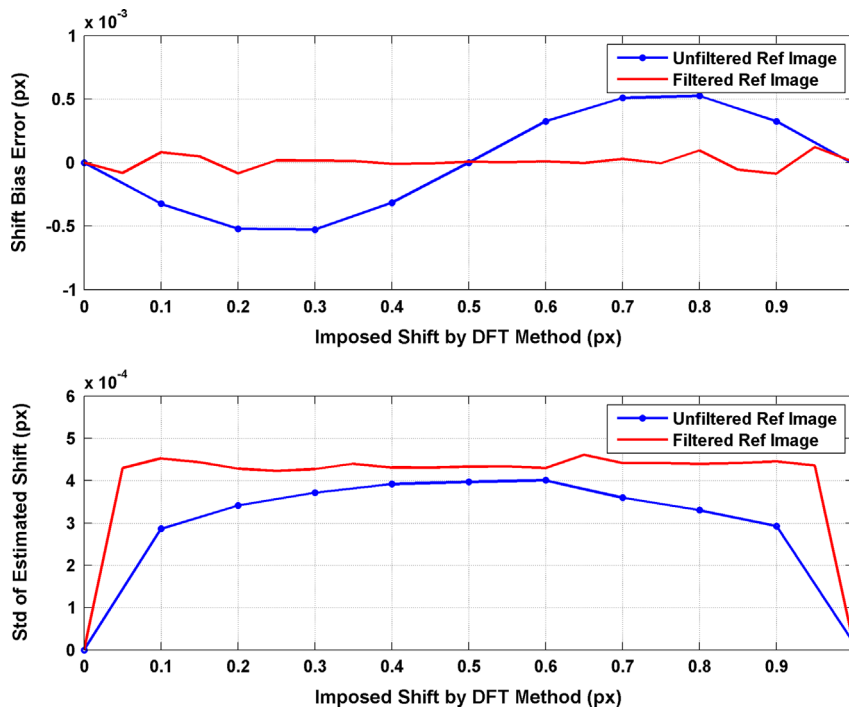

Fig. 2. Evaluation of DFT sub pixel shifting method, Bias Error or simply u–u_ref (up) and standard deviation of estimated shift (down).

performed on the generated images. In the current study Vic-2D software is used in order to perform the DIC analysis. The subset size and step were set equal to 21 and 7 pixel, respectively [7,8] (note that step of 7 pixel corresponds to an overlap of neighbor subsets equal to 14 pixel).

In Fig. 2, the Bias error i.e. the difference between the displacement estimated by DIC and the corresponding imposed shift value is shown versus the imposed rigid displacement. The periodic behavior of mean and standard deviation in the case of unfiltered image (Fig. 1(a)) is previously noticed and recognized in the literature [11,49,58] as it is a consequence of the 1 pixel periodicity of the properties of the image discretization process (assuming pixels on the sensor behave similarly) [58,59,60]. The amplitude of this systematic effect depends on image blurring, noise and the shift creating method itself. In this study, the chosen method for shifting is the one that, according to Reu [49] produces the minimum sub-pixel error, however image blurring and noise are still present. According to Fig. 2, applying the current method for generating

shifted images introduces an uncertainty less than 0.001 pixel. The shifting technique can therefore be used to develop the method to simulation the motion effect as described in Section 3.2.

It should be noted that the non-filter reference image represent a very particular case, which can be assumed as an almost ideal image, while the filtered one can be assumed as representative of a real acquired image, even if it is not affected by noise other than the discretization one. Due to this reason in the following of the paper the filtered reference image are used; only in Section 4.1 both the non-filtered and filtered images are considered for a comparison. The effect of the noise on numerical results is analyzed in the paper by adding Gaussian noise to the images, as described in Sections 4.2 and 4.3.

The kind of speckle images used in this analysis differ from the speckle pattern obtained with paint spray because the pattern was optimized to reduce the uncertainty according to the literature recommendations. In the case of spray-generated pattern the results of this analysis should be verified.

3.2. Generation of images with motion effect

As it was already discussed in Section 3.1, convolving the image with impulse function is a recognized method to simulate the sub pixel shifting, considering that the position of the impulse peek determines the value of imposed shift. In the case of dynamic conditions, the motion of the target during the exposure time is often not negligible. This phenomenon causes a motion effect (i.e. blurring) on the acquired images. In this paper we propose to apply an innovative technique, capable to recreate on a given speckle pattern, both the displacement and the blurring effect due to the motion of the measurement surface. The generated images will be used to test the performances of DIC in dynamic conditions.

Fig. 3 explains the approach using a simple example. A target is translating along the x axis and a frame is grabbed when the displacement is equal to 1 pixel. Under assumption of instantaneous acquisition, the acquired image would be just the same as the reference image but with a 1 pixel shift to the right and it can be simulated by convolving the reference image with the impulse function in Fig. 3(a). In this figure the impulse function is represented by $G(x)$. Considering now the scene recorded by means of a real camera, a given time is required for the camera to grab the frame. In this example, the target displaces half of a pixel during this exposure time. In order to simulate the acquired image in this case we suppose to generate several instantaneously acquired images during the exposure time and average them (Fig. 3(b)). If we increase the number of intermediate images up to infinity, we would get a square pulse with a width equal to the target's displacement during the exposure time also called simply as the stripe length (Fig. 3(c)). Based on this explanation, we propose to apply a motion effect simulation technique, which involves convolution of image with square pulse.

For explaining the motion effect simulation technique a brief review over the characteristics of square pulse and its Fourier transforms seems to be essential.

3.2.1. Motion effect simulation using square pulse

In scientific literature different methods are available to simulate the motion effect in digital images [61]; in this work a method based on the convolution of the original image with a rectangular pulse is implemented, applied and qualified to study the uncertainty of DIC in dynamic applications.

The square (rectangular) pulse $g(t)$, symmetric with respect to the time $t = 0$, can be defined as

$$g(t) = \text{rect}(t/w) = \begin{cases} 1 & \text{if } |t| < w/2 \\ 0 & \text{if } |t| > w/2 \end{cases} \tag{1}$$

Index 'w' is the parameter which indicates the width of the rectangle (i.e. the length of the stripe generated on the image).

The continuous Fourier transform of this function can be written as below [62]

$$G(f) = \int_{-\infty}^{\infty} \text{rect}(t/w) e^{-j2\pi ft} dt = w \frac{\sin(w\pi f)}{w\pi f} = w \sin c(wf) \tag{2}$$

In the case of dealing with a shifted square pulse (not centered) the Fourier transform is calculated as below

$$FT[g(t-a)] = FT[g(t)] \times \exp(-2i\pi fa) \tag{3}$$

where 'a' represents the time shift of the square pulse.

According to Eq. (2), the continuous Fourier transform of a square pulse is a sinc function. It is important to point out that, discrete Fourier transform of this pulse is not a sinc function and can be obtained starting from the discrete definition of the square pulse in time domain $x[n]$

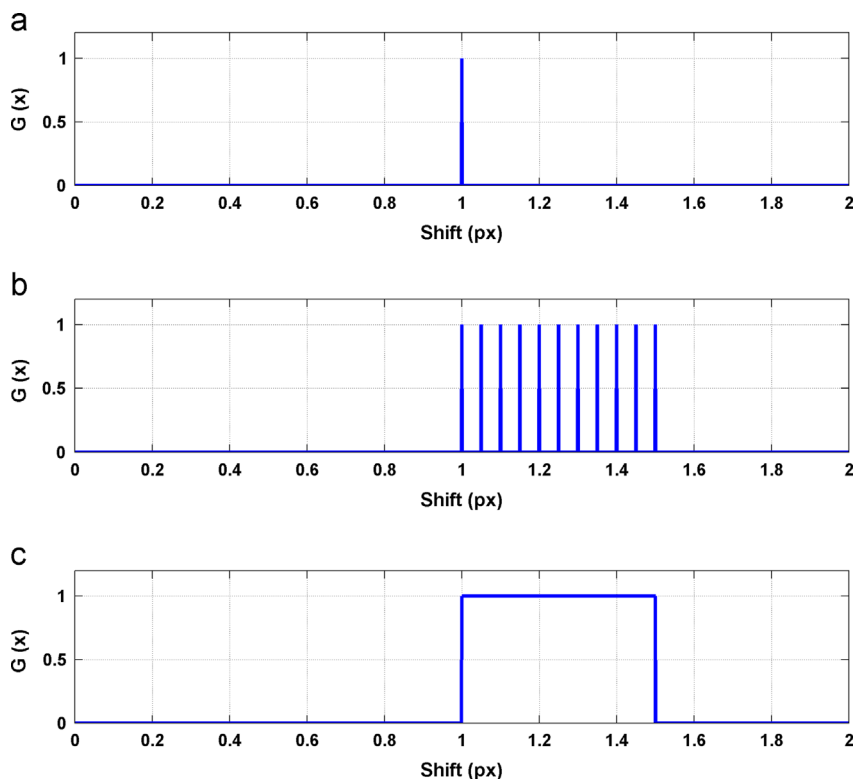$$x[n] = \begin{cases} 1 & 0 < n \leq N \\ 0 & \text{otherwise} \end{cases} \tag{4}$$

Fig. 3. Simulation of motion effect. Generation of a shifted image using a shifted impulse function (a), generation of several intermediate images using the corresponding shifted impulse function (b), simulation of motion effect using a square pulse (c).

DFT of the discrete square pulse $x[n]$ in [62]:

$$x(e^{j\omega}) = \sum_{-\infty}^{\infty} x[n]e^{-jn\omega} = \sum_{n=0}^{N-1} x[n]e^{-jn\omega}$$

$$= \frac{1-(e^{-Nj\omega})}{1-e^{j\omega}} = e^{-\frac{j\omega(N-1)}{2}} \times \frac{\sin(\omega N/2)}{\sin(\omega/2)} \tag{5}$$

Fig. 4, represents a square pulse signal with unitary width ($w=1$) and the corresponding discrete and continuous Fourier transform. Discrete and continuous Fourier transform of the square pulse will be used in the next subsections to simulate the motion effect.

3.2.2. Numerical method for motion effect simulation using DFT

According to the convolution theorem, the convolution in space domain is equivalent to multiplication in spatial frequency domain. The introduced technique to simulate the motion effect in horizontal direction is to calculate the DFT of each row of the image and multiply it by DFT of square pulse and finally calculate the inverse DFT of the product. Analogous procedure can be done
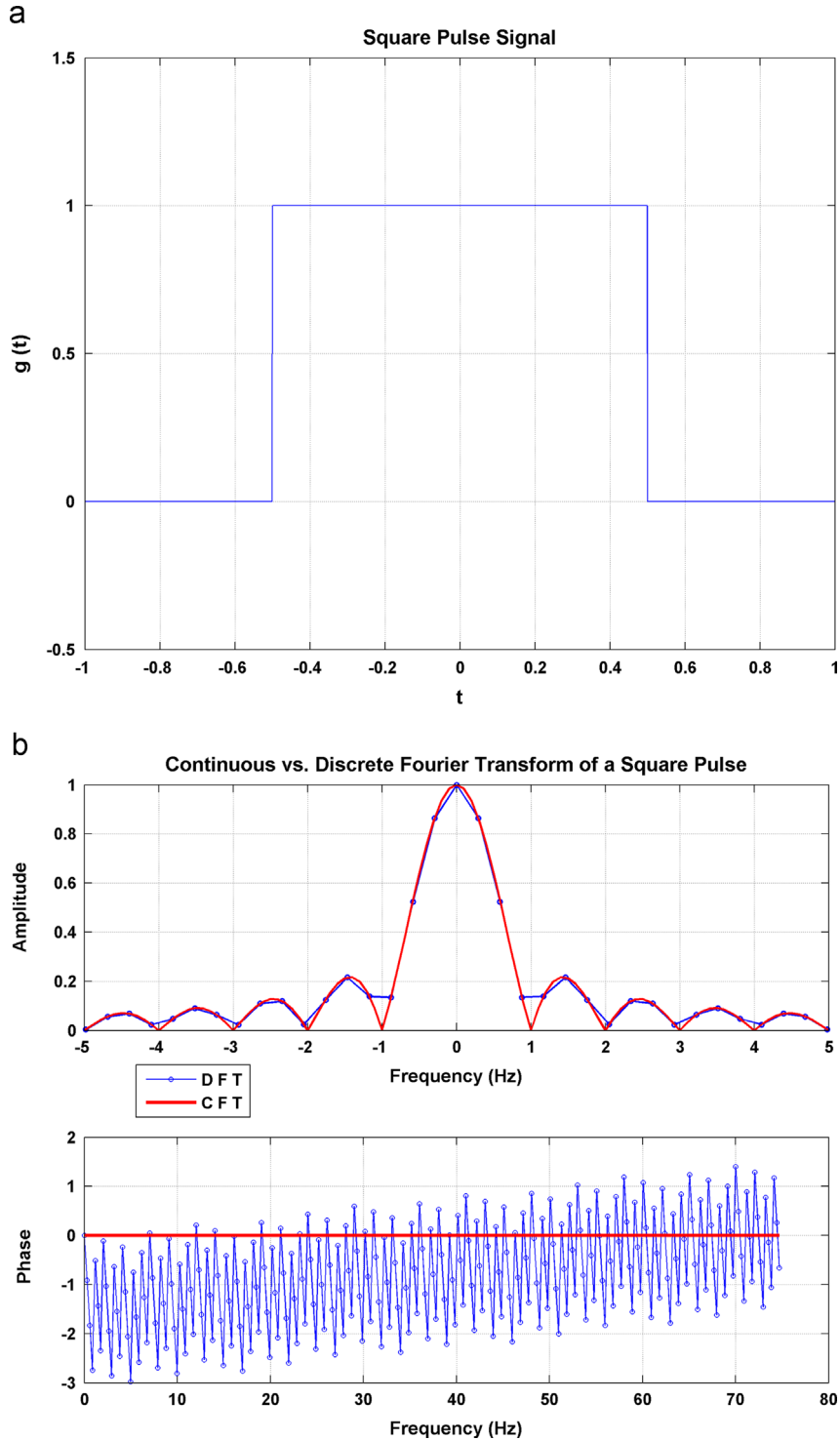

Fig. 4. A square pulse with $w=1$ (a) and corresponding continues and discrete Fourier transforms (b).

operating with image columns to simulate a vertical motion effect. We call this procedure, numerical method of motion effect simulation. It should be mentioned that if we convolve the image with shifted square pulse in space domain we will get a shifted image with motion effect.

3.2.3. Analytical method for motion effect simulation using DFT

The limitation for using the numerical method is that the square pulse length value can only accept the integer values but there is a need to simulate the motion with sub-pixel accuracy. Therefore the analytical method was proposed to be applied. Analytical method is based on creating the Fourier transform of the square pulse directly in frequency domain without the need to work in space domain; this will allow handling also motion effect with sub-pixel amplitude. The continuous Fourier transform of square pulse (i.e. sinc function) is directly multiplied by the DFT of each row of the reference image and the inverse DFT of the product is computed. An important issue regarding implementation of this method is to correctly define the frequency domain based on oddity or evenity of the signal length which has been addressed previously by Reu [49].

3.3. Generation of images with rigid motion effect

In order to apply the square pulse method the only concern is to obtain the equivalent shift and width of the square pulse corresponding to the motion or in the other words, to define values of parameters 'w' and 'a' in Eqs. (2) and (3). In the case of rigid motion, parameter 'a' can be easily defined since it represents the net displacement of the target with respect to the reference image. On the other hand 'w', is the length of the path covered by the target during an exposure time. For a given set of 'w' and 'a' parameters, the procedure explained in Section 3.2.3, can be readily implemented.

3.4. Simulation of acquired images in a sinusoidal vibration

In this section the introduced motion effect simulation method is implemented to simulate acquired images in the case of target moving with the sinusoidal vibration. The chosen speckle patterns are the ones previously presented in Fig. 1. Fig. 5 illustrates the implemented method to simulate ith image. The acquisition of the
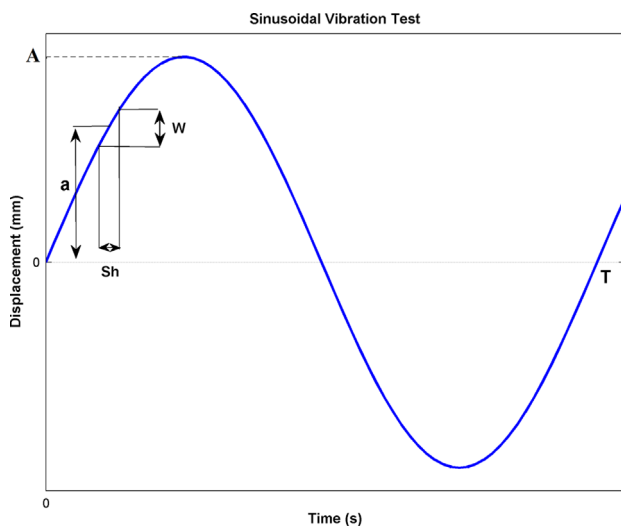

Fig. 5. Simulating the sinusoidal vibration test. Parameters 'A' and 'T' represent amplitude and period of the sinusoidal displacement law. Acquisition starts at $t=t_i$ and ends 'sh' (exposure time) seconds later at $t=sh+t_i$. Parameters 'a' and 'w' are considered as values of shift and motion effect index in generation of corresponding simulated image.

ith frame starts at $t=t_i$ and ends at $t=t_i+sh$, being sh an imposed shutter time of the camera. Assuming sh to be "small" with respect to the period of the sinusoidal waveform, the velocity within sh can be approximately considered constant. Under this hypothesis, the displacement of the target can be expressed as

$$\text{Target's displacement}: a = A \, \sin\left(\frac{2\pi}{T}(t_i+(sh/2))\right) \tag{6}$$

In which, A and T are respectively the amplitude (in millimeters) and the period of the displacement law (in seconds) and 'a' is the position of the target at $t=t_i+sh/2$ (position at the middle of the exposure time), (Fig. 5). On the other hand the displacement of the target during sh quantifies the width of the square pulse (w) introduced in Section 3.2.1. It can be simply written as

$$\text{Equivalent width of square pulse}: w = A\left[\sin\left(\frac{2\pi}{T}(t_i+sh)\right) - \sin\left(\frac{2\pi}{T}t_i\right)\right] \tag{7}$$

Now before substituting the calculated value of 'a' and 'w' from Eqs. (6) and (7) into Eqs. (2) and (3) these values should be converted into pixels using the camera scale factor. (The aim of this part was to implement Analytical method of motion effect simulation; the reason of this choice has been already discussed in Section 3.2.3).

It is worth to stress that the imposed displacement in the simulated image is equal to 'a', i.e. the displacement of the target at $t=t_i+sh/2$ (displacement at the middle of the exposure time).

Consequently, once the sampling frequency of the image acquisition hardware and its shutter time are defined, it is possible, for a given sinusoidal motion law, to numerically generate a sequence of frames as expected to be captured by the camera starting from a single image of the speckle pattern acquired in static condition.

The images generated with both rigid motion technique (Section 3.3) and sinusoidal motion (Section 3.4) are available for download at Ref. [63] for possible analysis of other authors.

3.5. Experiments

In the second part of the study, in order to validate the developed simulation model, several experimental tests were carried out on a vertically vibrating planar target with a speckle pattern on it, in different frequencies and amplitudes using an LSD shaker (V830-335TRUNNION, with maximum frequency of 3 kHz, maximum mass of 12 kg and maximum sinusoidal speed of 2.0 m/s). The frequency of motion was increased from 5 to 10, 15 and 20 Hz and the amplitude of shaker was changed from 0.5 mm (1.5 pixel) to 1.5 mm (4.5 pixel), 3 mm (9 pixel), 5 mm (15 pixel) and 7 mm (21 pixel).

The speckle pattern was printed with high quality laser printer and was stuck on a support that does not show the natural frequencies in the frequency ranges interested by the test. Then, it was being captured by a camera (AVT Marlin F131B, equipped with a 280×1024 CMOS sensor and a lens with a nominal focal length of 16 mm) with frame rate of 11, 16, 20 or 21 depending on the specific test (due to the limited frame rate of the used camera (25 fps at full resolution), the tests were done in controlled aliasing condition). A laser interferometer (single point Polytec Scanning Vibrometer PSV300laser interferometer with resolution of 2.56 μm), was used as the reference values for target's position. Fig. 6 shows one cycle of the motion as acquired by the camera, starting from the static position. The speckle pattern was square shaped with size of 100 mm (300 pixel) and average grain size of

4 pixel. The motion effect is more visible in neutral position where the velocity is maximum (Fig. 6).

4. Results and discussion

This section starts with DIC analysis of numerically generated images with motion effect. Then the effect of adding noise to this group of images is investigated. Next, the acquired images of sinusoidal vibration in few cases were simulated by the introduced technique and the uncertainties of the measurements were estimated using DIC analysis. In order to validate the model, the results of experiments were compared with that of the simulations. At last, further assessments of DIC uncertainty were performed in the case of experimental tests.

4.1. DIC analysis of images with rigid motion effect

In the current study Vic-2D software is used in order to perform the DIC analysis. The subset size and step were set equal to 21 and 7 pixel, respectively [7,8]. Fig. 7 illustrates portions of the generated images with an increasing motion effect w in the case of rigid motion. The pattern degradation is quite evident; for a quantitative analysis of pattern quality, the mean intensity gradient (MIG) was proposed by Pan et al. and proved to be closely related to both mean bias error and standard deviation of the measured displacement [64]. MIG is computed as the average of the squared gray level gradients normalized by the size of the image. As a first index of motion effect on DIC uncertainty the MIG values of each image is computed and mentioned in Fig. 7. As can be seen increasing w the MIG values drop, showing that the expected uncertainty grows. This prediction is confirmed by the DIC analysis described in the following.

By performing DIC analysis on the generated images with respect to the original one the displacement and strain value of every subset was obtained. These values have been computed over the whole image and the result is reported in Fig. 8, in terms of mean and standard deviation of the discrepancy between the imposed and estimated motion. In Fig. 8 only the result for $w \leq 8$,

is shown because the digital image correlation method is barely able to detect the pixels in the generated image with w index higher than 8.

At first (results shown in Fig. 8), the reference displacement has been set equal to zero in both horizontal and vertical directions and motion effect i.e. blurring, has been applied along the vertical direction. The discrepancy standard deviation can be noticed to be about one order of magnitude bigger than the discrepancy average and it can consequently been considered a reliable estimation of the measurement uncertainty. Therefore, it can be claimed that the uncertainty is the meaningful quantity (not mean) that should be taken into account. According to Fig. 8, in all cases it increases faster as 'w' increases.

In order to investigate DIC performances in the case of rigid motion when the net displacement is not equal to zero, sub pixel shifting method, discussed in Section 3.1, is applied on the two reference images shown in Fig. 1. Fig. 9, represents the results in the case of shifting an image with an imposed motion effect of $w=7$ (to simulate a condition of a strong motion effect).

According to this figure, bias error and standard deviation of the estimated shift both show an overall constant trend with small fluctuations around their corresponding value obtained in the case of zero displacement (Fig. 8). Moreover, the bias and the standard deviation of the shift reported in Fig. 9 (the case of combined imposed shift and imposed motion effect $w=7$) are much larger than the corresponding ones in Fig. 2 (the case of imposed shift with zero imposed motion effect). This is due to the simulated motion effect ($w=7$) and can prove that the uncertainty of result mainly depends on the motion effect while the imposed shifting value has a negligible effect.

4.2. Effect of adding Gaussian noise to the generated images

In this section a Gaussian noise in two levels was added to the generated images before applying the DIC analysis in order to check if this changes the uncertainty in some way. Fig. 10 shows the mean and standard deviation of displacement and strain after adding noise to the images. Noise level1 and level2 are two zero
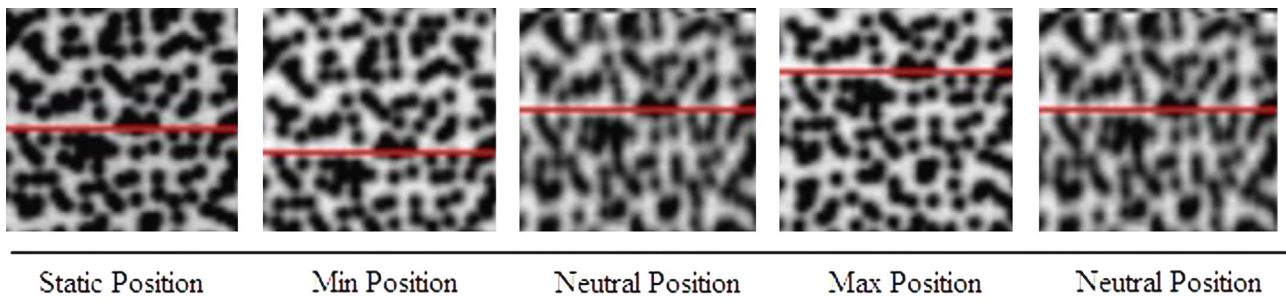

| Static Position | Min Position | Neutral Position | Max Position | Neutral Position |

Fig. 6. A part of a typical image taken by the camera in one cycle of the motion starting and ending in static position. The red horizontal line is sketched to give better understanding of the sinusoidal vibration. (For interpretation of the references to color in this figure legend, the reader is referred to the web version of this article.)
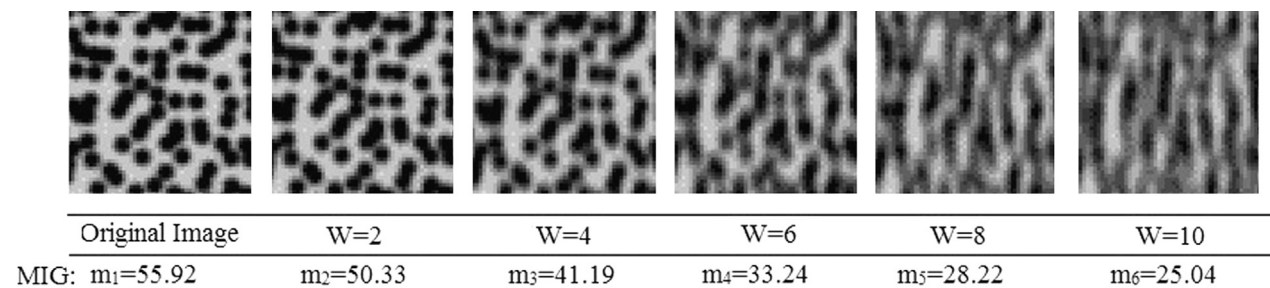

	Original Image	W=2	W=4	W=6	W=8	W=10
MIG:	$m_1=55.92$	$m_2=50.33$	$m_3=41.19$	$m_4=33.24$	$m_5=28.22$	$m_6=25.04$

Fig. 7. Portions of the generated images with an increasing motion effect w in the case of rigid motion and the corresponding mean intensity gradient (MIG).
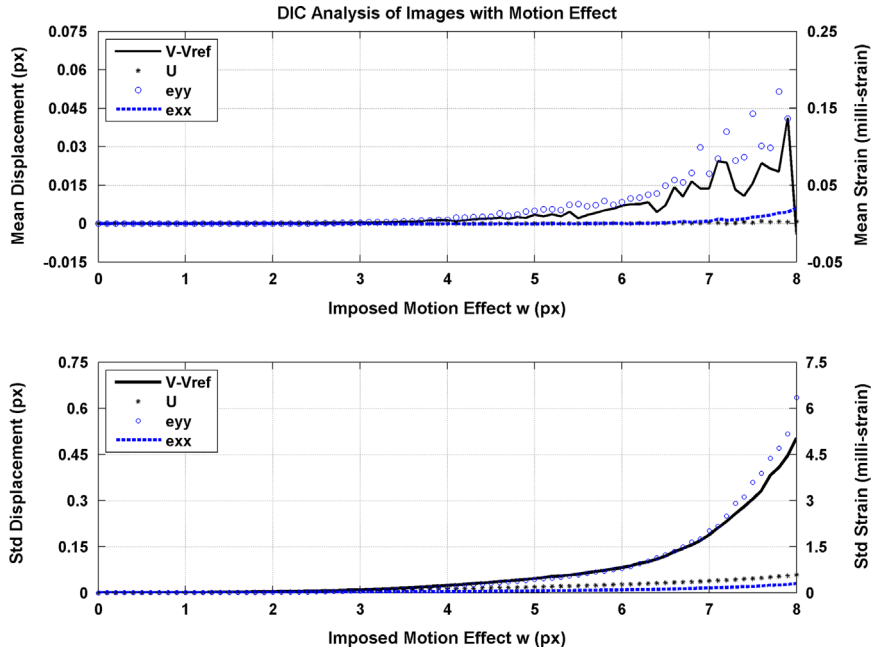
Fig. 8. Mean and standard deviation of displacement and strain in the case of rigid motion with zero displacement (V and eyy are respectively the displacement and strain in the direction of Motion. U and exx are displacement and strain in the opposite direction).
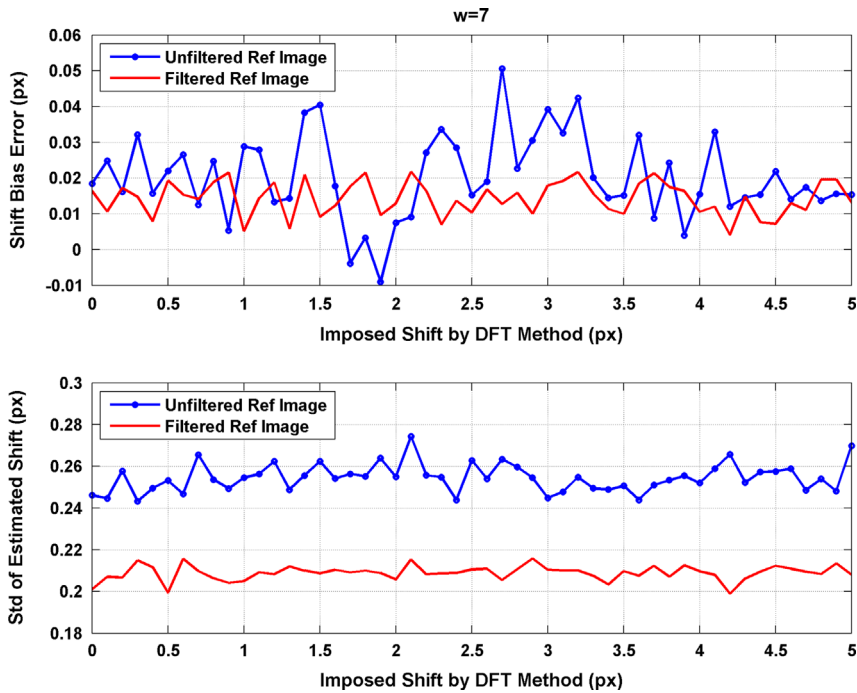

Fig. 9. DIC results in the case of rigid motion with $w=7$ and non-zero displacement.

mean Gaussian noises with standard deviation of 5 and 10 Gy levels, respectively (8 bit images are considered in this work). The reference displacement is equal to zero in both horizontal and vertical directions but the motion effect (stripe) is simulated in vertical direction. Note that the mean and standard deviation curves of both displacement and strain are very similar in Fig. 8 (no noise) and Fig. 10, where the images are corrupted by noise. This proves that, although adding Gaussian noise to the image affects the bias and random error, the blurring due to motion increases the uncertainty much more than the noise and therefore the results are nearly independent by the noise level.

4.3. Simulation of sinusoidal vibration and experimental validation

In this section, the introduced simulation technique was implemented on the planar target with sinusoidal vibration. The procedure of image generation is already revealed in Section 3.4. As the next step, the simulated image set is analyzed with the DIC technique and the discrepancy between the imposed and the estimated time histories is utilized to estimate the uncertainty. Table 1 represents the specifications of the simulated sinusoidal vibration cases. The last column is the 'maximum nominal stripe length' which can be defined as is the length that the target
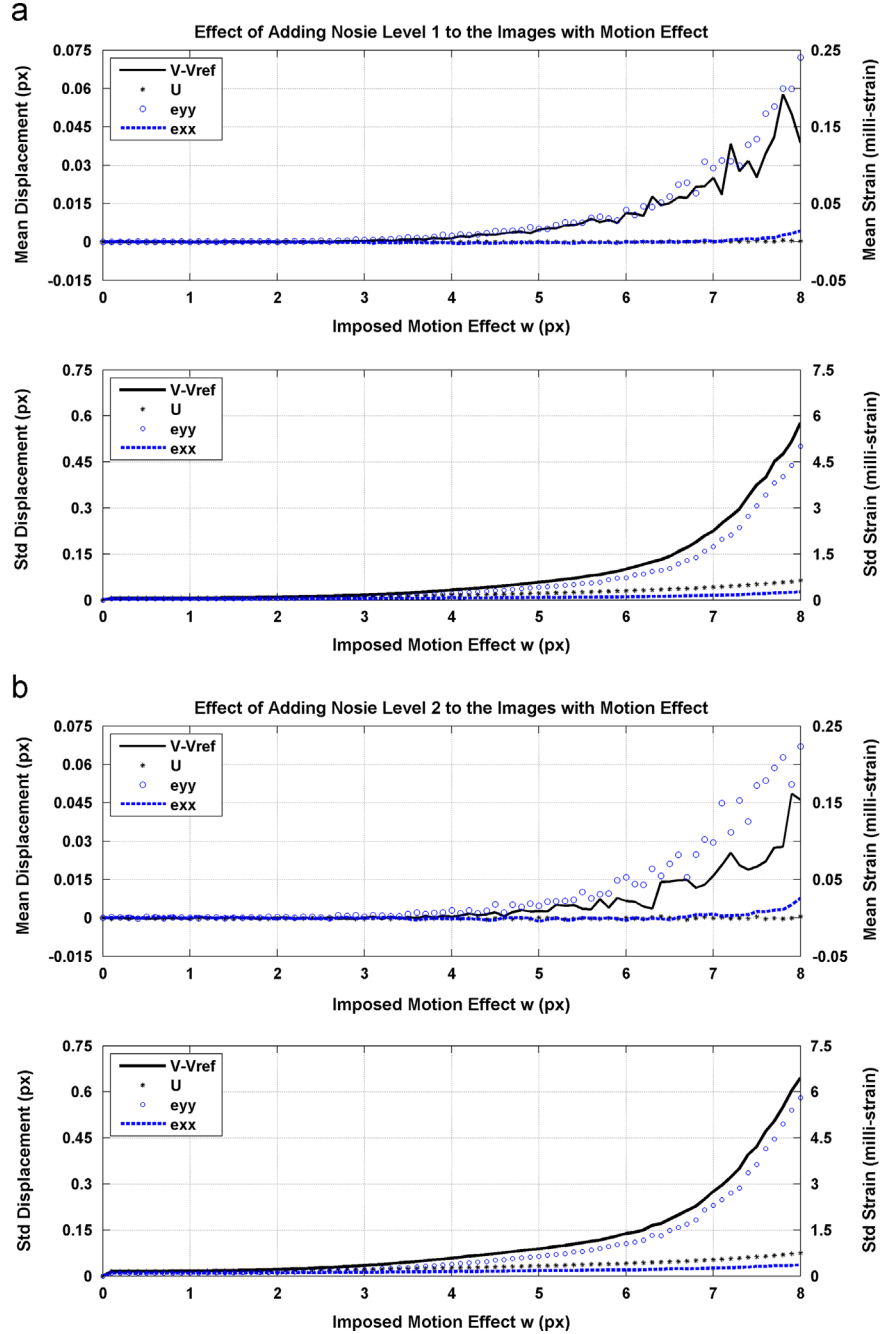
Fig. 10. Mean and standard deviation of displacement in the case of rigid motion with zero displacement after adding noise with level one (a) and with level two (b) (V and eyy are respectively the displacement and strain in the direction of Motion. U and exx are displacement and strain in the opposite direction).

displaces during an exposure time (or simply the stripe length) if it has the maximum speed the whole interval. It is calculated as below:

$$\text{Max Nominal Stripe Length} = \text{Max speed} \times sh = 2\pi fA \times sh \qquad (8)$$

In which, 'f' and 'A' are respectively the nominal frequency (in hertz) and amplitude (in millimeters) of the specific test and 'sh' is the exposure time (shutter time in seconds).

It should be emphasized that this motion effect simulation method works under the hypothesis of constant target velocity during the camera exposure time. Due to this reason, as the ratio between the exposure time and the target motion period increases, an increasing approximation is introduced in the generated images (see Fig. 5). Therefore, the parameters of the

simulated cases where designed in a way that this ratio does not exceed 7.5% (Test number 4 in Table 1). Aiming to recreate the conditions of real tests some levels of noise was added to the images.

In order to validate the results of simulations, the simulated cases were also experimentally tested. The specifications of the experimental set up are already explained in Section 3.5. In this case, DIC estimated displacements were compared with the corresponding values measured by the laser interferometer. The result is reported in terms of discrepancy which has been defined as the difference between time histories of the displacement estimated by DIC and reference displacement (measured by laser interferometer) (Fig. 11). Note that the discrepancy calculated here is a point-by-point difference; since the interferometer and camera had different reference systems, before comparing the

Table 1
Specifications of simulated tests.

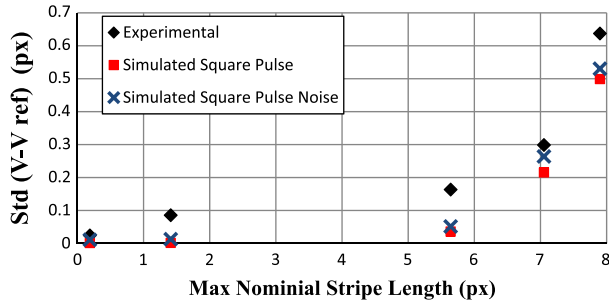| Test number	Amplitude (pixel)	Frequency (Hz)	Exposure time (ms)	Frame rate (frame/s)	Exposure time(s)/ period(s)	Max nominal strip length (pixel)
1	1.5	5	4	20	0.02	0.1881
2	9	5	5	20	0.025	1.4104
3	9	5	20	20	0.05	5.6417
4	15	5	15	20	0.075	7.0521
5	21	15	4	16	0.06	7.8983

Fig. 11. Simulation of few sinusoidal vibration tests and the corresponding experimental validation. The vertical axis is the standard deviation of discrepancy.
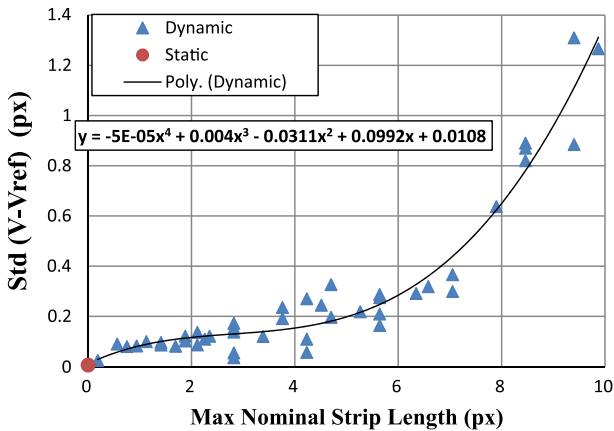

Fig. 12. Standard deviation of discrepancy with respect to max nominal stripe length in real tests.

two time histories the mean of the two signals were set to zero. Therefore, the mean value of the discrepancy is zero by definition and is not reported here. Fig. 11 represents the standard deviation of discrepancy.

In Fig. 11, the simulated result obtained after adding noise to the images is also plotted. The noise was a zero mean Gaussian noise with standard deviation of 2.5. This level of noise was a reasonable value considering the acquisitions in the real tests.

The discrepancies between numerical simulation and experimental tests can be due the fact that the synthetic speckle of the target in the simulated images was generated without reproducing the behavior of a real optics and image sensor combination, while the actual images acquired with the camera are corrupted by the fill factor of the sensor and possible brightness and contrast variation due to experimental conditions. Nevertheless Fig. 11 shows a good agreement between the simulations and the experiments.

4.4. Experimental uncertainty in estimation of the vibration

Further experimental tests were conducted aiming to assess the uncertainty of DIC in the estimation of the instantaneous position of the target during harmonic motion. The results again are reported in terms of the standard deviation of discrepancy reminding that the mean of discrepancy is zero by definition. In Fig. 12, the results of more than 40 cases of harmonic vibration tests are reported.

Fig. 12 represents a quadratic polynomial fit for the test results. The value of vertical axis offset is equivalent to the DIC displacement uncertainty in static condition. This value has been reported in Ref. [65], to be equal to 0.006 pixel (circular marker). This graph proves that, our estimated trend is in a great agreement also with the results of that study.

5. Conclusion

Dealing with a moving target in dynamic conditions, causes a motion effect (i.e. blurring) on the acquired images. This factor is an important source of uncertainty that needs to be quantified. In the present study systematic uncertainty assessment of DIC method in general dynamic applications was done.

In the first part of the work, a method to simulate the motion effect on a reference image was proposed to be applied. This method allows us to simulate the acquired images in a real dynamic test and estimate the measurement uncertainty caused by the motion effect in fully controlled conditions. Using this technique, the uncertainty of DIC measurement was estimated. The images generated with the technique proposed in this work are available for download at [63].

The second part of the study validated the simulation technique by experimentally reconstructing the simulated cases. Therefore, the corresponding harmonic motion was imposed to a target, while it was captured by a camera and it is position was measured by a laser interferometer. The results show good agreement between the experiments and the simulations. After conducting further experimental tests, the DIC uncertainty in estimation of the amplitude of the sinusoidal vibration was also assessed.

Providing known testing condition (in particular the relation between target velocity and camera shutter time), the presented method can consequently be exploited to quantify the motion induced uncertainty in dynamic DIC measurements simply starting from a reference unblurred image of the measurement surface.

DIC can also be used to estimate the strain over a certain gauge length, for example in the case of cyclic fatigue tests; in these cases the uncertainty associated to the mean strain value is of interest. Considering for example a gauge test of 50 pixel, an uncertainty of 0.2 pixel on the displacement estimation (corresponding to $w=7$, see Fig. 8) leads a maximum uncertainty in strain of 0.8%, which is usually not acceptable. This is however a very critical condition of 7 pixel motion during exposure time; by reducing the exposure time of a factor of 2 the stripe length becomes $w=3.5$ pixel (still representing a non-negligible blurring effect) and the corresponding uncertainty becomes 0.02 pixel. The uncertainty on the strain becomes accordingly 0.08%.

References

[1] Cloud G. Optical methods of engineering analysis. 1st ed. Cambridge: Cambridge University Press; 1998.

[2] Rastogi PK. Photomechanics. 1st ed. Springer; 2000.

[3] Vautrin A, Lee J, Molimard J, Surrel Y. Full-field optical techniques: applications to strain measurement and mechanical identification. In: Proceedings of the 10th European conference on composite materials. (ECCM10), Bruges, Belgium; 2002.

[4] Surrel Y. Full-field optical methods for mechanical engineering: essential concepts to find one's way. In: Proceedings of the second international conference on comp sites testing and model identification. Bristol, U.K; 2004.

[5] Grediac M. The use of full-field measurement methods in composite material characterization: interest and limitations. Composites Part A 2004;35:751–61.

[6] Sharpe J, William N. Springer handbook of experimental solid mechanics. Springer; 2007.

[7] Sutton MA, Orteu JJ, Schreier HW. Image correlation for shape, motion and deformation measurements: basic concepts, theory and applications. Springer; 2009.

[8] Pan B, Qian K, Xie H, Asundi A. Two-dimensional digital image correlation for in-plane displacement and strain measurement: a review. Meas Sci Technol 2009;20:062001.

[9] Schmidt T, Tyson J, Galanulis K. Full-field dynamic displacement and strain measurement using advanced 3D image correlation photogrammetry. Exp Tech 2003;27(3):47–50.

[10] Wang X, Yi T, Tang Q, Feng L, Ni G, Zhou L. Simulation and analysis of vibration blurred images. In: Proceedings of wireless communications networking and mobile computing IEEE; 2010. p. 1-4.

[11] Schreier HW, Sutton MA. Systematic errors in digital image correlation due to undermatched subset shape functions. Exp Mech 2002;42(3):303–10.

[12] Holst GC. CCD arrays, cameras, and displays. 2nd ed. Washington: Bellingham: SPIE Optical Engineering Press; 1998.

[13] Roux S, Hild F. Stress intensity factor measurements from digital image correlation: post-processing and integrated approaches. Int J Fract 2006;40:141–57.

[14] Besnard G, Hild F, Roux S. Finite-element displacement fields analysis from digital images: application to Portevin–Le Châtelier bands. Exp Mech 2006;46(6): 789–803.

[15] Wang ZY, Li HQ, Tong JW, Ruan JT. Statistical analysis of the effect of intensity pattern noise on the displacement measurement precision of digital image correlation using self-correlated images. Exp Mech 2007;47:701–7.

[16] Wang YQ, Sutton MA, Reu PL, Miller TJ. Image matching error assessment in digital image correlation. In: Proceedings of the SEM annual conference. Albuquerque New Mexico, USA; 2009.

[17] Wang YQ, Sutton MA, Bruck HA, Schreier HW. Quantitative error assessment in pattern matching: effects of intensity pattern noise, interpolation, strain and image contrast on motion measurements. Strain 2009;45:160–78.

[18] Um GJ, Kim H. Experimental error assessment for image correlation analysis on a paper tensile specimen. J Ind Eng Chem 2007;13(2):214–8.

[19] Siebert T, Becker T, Spiltthof K, Neumann I, Krupka R. High-speed digital image correlation: error estimations and applications. Opt Eng 2007;46(5):051004.

[20] Tiwari V, Sutton MA, McNeill SR. Assessment of high speed imaging systems for 2D and 3D deformation measurements: methodology development and validation. Exp Mech 2007;47:561–79.

[21] Haddadi H, Belhabib S. Use of rigid-body motion for the investigation and estimation of the measurement errors related to digital image correlation technique. Opt Lasers Eng 2008;46:185–96.

[22] Lava P, Van Paepegem W, Coppieters S, De Baere I, Wang Y, Debruyne D. Impact of lens distortions on strain measurements obtained with 2D digital image correlation. Opt Lasers Eng 2013;51(5):576–84.

[23] Pan B, Yu L, Wu D, Tang L. Systematic errors in two-dimensional digital image correlation due to lens distortion. Opt Lasers Eng 2013;51(2):140–7.

[24] Reu PL, Sutton MA, Wang Y, Miller TJ. Uncertainty quantification for digital image correlation. In: Proceedings of the SEM annual conference. Albuquerque New Mexico USA; 2009.

[25] Pan B, Qian K, Xie H, Asundi A. On errors of digital image correlation due to speckle patterns. In: Proceedings of the international conference on experimental mechanics; 2008. p. z1:z7.

[26] Crammond G, Boyd SW, Dulieu-Barton JM. Speckle pattern quality assessment for digital image correlation. Opt Lasers Eng 2013;51(12):1368–78.

[27] Bornert M, Brémand F, Doumalin P, Dupre JC, Fazzini M, Grediac M, et al. Assessment of digital image correlation measurement errors: methodology and results. Exp Mech 2009;49(3):353–70.

[28] Fazzini M, Mistou S, Dalverny O, Robert L. Study of image characteristics on digital image correlation error assessment. Opt Lasers Eng 2010;48:335–9.

[29] Lava P, Cooreman S, Coppieters S, De Strycker M, Debruyne D. Assessment of measuring errors in DIC using deformation fields generated by plastic FEA. Opt Lasers Eng 2009;47:747–53.

[30] Lava P, Coppieters S, Wang Y, Van Houtte P, Debruyne D. Error estimation in measuring strain fields with DIC on planar sheet metal specimens with a non-perpendicular camera alignment. Opt Lasers Eng 2011;49:57–65.

[31] Lava P, Cooreman S, Debruyne D. Study of systematic errors in strain fields obtained via DIC using heterogeneous deformation generated by plastic FEA. Opt Lasers Eng 2010;48:457–68.

[32] Wang Y, Lava P, Coppieters S, De Strycker M, Van Houtte P, Debruyne D. Investigation of the uncertainty of DIC under heterogeneous strain states with numerical tests. Strain 2012;48(6):1–10.

[33] Zhou Y, Sun C, Chen J. Adaptive subset offset for systematic error reduction in incremental digital image correlation. Opt Lasers Eng 2014;55:5–11.

[34] Wang YQ, Sutton MA, Ke XD, Schreier HW, Reu PL, Miller TJ. On error assessment in stereo-based deformation measurements Part I: Theoretical developments for quantitative estimates. Exp Mech 2011;51:405–22.

[35] Ke XD, Schreier HW, Sutton MA, Wang YQ. Error assessment in stereo-based deformation measurements Part II: Experimental validation of uncertainty and bias estimates. Exp Mech 2011;51:423–41.

[36] Hu Z, Xie H, Lu J, Wang H, Zhu J. Error evaluation technique for three-dimensional digital image correlation. Appl Opt 2011;50(33):6239–47.

[37] Schmidt T, Tyson J, Galanulis K. Full-field dynamic displacement and strain measurement—specific examples using advanced 3D image correlation photo-grametery: Part1. Exp Tech 2003;26:47–50.

[38] Schmidt T, Tyson J, Galanulis. Full-field dynamic displacement and strain measurement—specific examples using advanced 3D image correlation photo-grametery: Part 2. Exp Tech 2003;27:22–6.

[39] Kirugulige MS, Tippur HV, Denney TS. Measurement of transient deformations using digital image correlation method and high-speed photography: application to dynamic fracture. Appl Opt 2007;46(22):5083–96.

[40] Wang W, Mottershead JE, Mares C. Vibration mode shape recognition using image processing. J Sound Vib 2009;326:909–38.

[41] Siebert T, Wood R, Splitthof K. High speed image correlation for vibration analysis. J Phys Conf Ser 2009;181:1–8.

[42] Siebert T, Crompton MJ. Application of high speed digital image correlation for vibration mode shape analysis. In: Proceedings of the SEM annual conference. Indianapolis, Indiana USA; June 2010.

[43] Wang W, Mottershead JE, Ihle A, Siebert T, Reinhard Schubach H. Finite element model updating from full-field vibration measurement using digital image correlation. J Sound Vib 2011;330:1599–620.

[44] Helfrick MN, Niezrecki C, Avitabile P, Schmidt T. 3D digital image correlation methods for full-field vibration measurement. Mech Syst Sig Process 2011;25:917–27.

[45] Warren C, Niezrecki C, Avitabile P, Pingle P. Comparison of FRF measurements and mode shapes determined using optically image based, laser, and accel-erometer measurements. Mech Syst Sig Process 2011;25:2191–202.

[46] Wang W, Mottershead JE, Siebert T, Pipino A. Frequency response functions of shape features from full-field vibration measurements using digital image correlation. Mech Syst Sig Process 2012;28:333–47.

[47] Ha NS, Jin T, Goo NS. Modal analysis of an artificial wing mimicking an Allomyrina dichotoma beetle's hind wing for flapping-wing micro air vehicles by noncontact measurement techniques. Opt Lasers Eng 2013;51(5):560–70.

[48] Reu PL. Experimental validation of 2D uncertainty quantification for digital image correlation. In: Proceedings of the EPJ web of conferences; 2010. vol. 6, 31003.

[49] Reu PL. Experimental and numerical methods for exact subpixel shifting. Exp Mech 2011;51:443–52.

[50] Wattrisse B, Chrysochoos A, Muracciole JM, Némoz-Gaillard M. Analysis of strain localization during tensile tests by digital image correlation. Exp Mech 2000;41:29–39.

[51] Zhou P, Goodson KE. Sub-pixel displacement and deformation gradient measurement using digital image/speckle correlation (DISC). Opt Eng 2001;40:1613–20.

[52] Pan B, Xie HM, Xu BQ, Dai FL. Performance of sub-pixel registration algorithms in digital image correlation. Meas Sci Technol 2006;17:1615–21.

[53] Sousa AMR, Xavier J, Vaz M, Morais JJL, Filipe VMJ. Cross-correlation and differential technique combination to determine displacement fields. Strain 2011;47:87–98.

[54] Zhang J, Cai Y, Ye W, Yu TX. On the use of the digital image correlation method for heterogeneous deformation measurement of porous solids. Opt Lasers Eng 2011;49:200–9.

[55] Orteu JJ, Garcia D, Robert L, Bugarin F. A speckle texture image generator, In: Speckle06: speckles, from grains to flowers; 2006. p. 63410H-63410H.

[56] Chen J, Jin G, Meng L. Applications of digital correlation method to structure inspection. Tsinghua Sci Technol 2007;12:237–43.

[57] Niezrecki C, Avitabile P, Warren C, Pingle P, Helfrick M. A review of digital image correlation applied to structural dynamics. In: Proceedings of AIP conference; 2010. vol. 1253. p. 219-232.

[58] Schreier HW, Braasch JR, Sutton MA. Systematic errors in digital image correlation caused by intensity interpolation. Opt Eng 2000;39(11):2915–21.

[59] Sutton MA, McNeill SR, Jang J, Babai M. Effects of subpixel image restoration on digital correlation error estimates. Opt Eng 1988;27:870–7.

[60] Choi S, Shah SP. Measurement of deformations on concrete subjected to compression using image correlation. Exp Mech 1997;37:307–13.

[61] Gonzalez RC, Woods RE. Digital image processing. 2nd ed. New York: Prentice-Hall Inc; 2002.

[62] Briggs WL, Henson VE. The DFT: an owner's manual for the discrete Fourier transform, society for industrial and applied mathematics, Philadelphia, 1995.

[63] ⟨http://people.mecc.polimi.it/zappa/DIC⟩.

[64] Pan B, Lu Z, Xie H. Mean intensity gradient: an effective global parameter for quality assessment of the speckle patterns used in digital image correlation. Opt Lasers Eng 2010;48:469–77.

[65] Paolo Mazzoleni. Uncertainty estimation and reduction in digital image correlation measurements [Doctoral Dissertation]. Politecnico di Milano, XXV cycle; 2013.